Distributed Formation Control and Navigation of Fixed-wing UAVs at Constant Altitude

Kaveh Fathian, Tyler H. Summers, Nicholas R. Gans

***Abstract*— We present a distributed control strategy for a team of fixed-wing Unmanned Aerial Vehicles (UAVs), such that they achieve a desired formation and travel along a desired direction at a constant altitude. We describe the motion of UAVs with the kinematic unicycle model, and impose the constraints that the airspeed and turning rate of UAVs must satisfy some practical bounds. Based on this model, a control strategy is proposed, and local convergence of the team to the desired formation and travel direction is proved. The control direction returned by our strategy is well-suited as a high-level motion planning input to a low-level UAV autopilot, which can compensate for the aerodynamics, wind effects, disturbances, etc., that are not accounted for in the unicycle model. The proposed strategy is fully distributed and can be implemented using relative position measurements acquired by UAVs in their local coordinate frames. Furthermore, UAVs do not need to communicate. Simulations are provided to typify the proposed strategy.**

***Index Terms*— Unmanned aerial vehicles, multi-agent system, distributed formation control.**

Supplementary Material

Video of the simulations is available at https://youtu.be/fCpwfsnTVNY, and the simulation code can be accessed at https://goo.gl/QH5qhw.

I. Introduction

In recent years, the Unmanned Aerial Vehicle (UAV) technology has reached a level of maturity that it is now possible to deploy hundreds of UAVs in a mission. The large number of deployed vehicles allows a team of small, inexpensive UAVs to efficiently execute missions such as search and rescue [1], [2], inspection [3], [4], and surveillance [5]. In these applications, the ability to fly the team of UAVs from one waypoint to another is the fundamental building block upon which more sophisticated navigation capabilities can be built.

As the number of deployed UAVs increases, controlling agents from a command center becomes less practical. This is due to the limited communication bandwidth, which becomes saturated as the number of agents increases. Furthermore, the centralized control lacks resilience to communication loss, hardware failure, and malicious attacks such as jamming or spoofing of the communication signal. Hence, UAVs in large teams should have a level of autonomy to individually plan their motion in accordance with the team to perform the desired task. To navigate the UAVs between waypoints, distributed formation control techniques can be employed, where the UAVs autonomously achieve a desired formation and travel toward the desired destination (e.g., see Fig. 1).

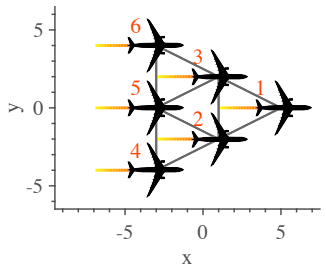

Fig. 1. A team of UAVs moving in triangle formation along the positive x-direction.

In this work, we propose a distributed guidance strategy to navigate a team of fixed-wing UAVs at a constant altitude toward a desired waypoint. Our strategy is based on using the unicycle kinematic model for UAVs' motion, where the airspeed and turning rate of UAVs must satisfy practical bounds known as the Dubins constraints [6]. Given a set of control gains and a desired destination, which can be communicated to the agents before the mission, onboard sensor measurements of each UAV can be used to compute a control direction. This control is well-suited as a high-level motion planning input to a low-level UAV autopilot, which can compensate for the aerodynamics, wind effects, disturbances, etc., that are not accounted for in the unicycle model. Advantages of the proposed strategy over centralized methods include better scalability, naturally parallelized computation, resilience to communication loss and hardware failure, and robustness to uncertainty and lack of global knowledge. In particular, the UAVs can achieve the formation using only the local relative position measurements of their neighbors, and without communicating with each other. This increases the stealth and robustness of the team to jamming. Simulations are presented to typify the performance of the proposed strategy.

The distributed formation control used in this work is inspired by [7], [8], where a linear control for agents with single-integrator model is developed. Extension of the formation control strategy to the UAVs' unicycle model is inspired by [9], [10], where application of gradient-descent control strategies to agents with nonholonomic motion constraints have been studied. Unlike the aforementioned work, and

*This work was supported in part by the OSD Sponsored Autonomy Research Pilot Initiative, RW Autonomy Initiative, and U.S. Air Force Research Laboratory under Grant FA8651-17-1-0001.

K. Fathian and N. R. Gans are with the Department of Electrical Engineering, T. H. Summers is with the Department of Mechanical Engineering, University of Texas at Dallas, Richardson, TX, 75080 USA. E-mail: {kaveh.fathian, tyler.summers, ngans}@utdallas.edu.

our previous work on formation control [11], [12] where the desired formation is stationary, here the agents should achieve the formation while moving toward a destination. This, together with the unicycle dynamics with Dubins constraints are the main novelties of this paper.

The organization of the paper is as follows. The notation and assumptions used in the paper are introduced in Section II. In Section III, the control law for single-integrator agents is introduced, and an optimization problem to find stabilizing control gains is presented. In Section IV, unicycle kinematic model with Dubins constraint is introduced, and the formation control is applied to this model. Simulations are presented in Section V, followed by concluding remarks in Section VI.

II. Notation and Assumptions

We consider a team of $n \in \mathbb{N}$ vehicles and describe the sensing topology among agents by an undirected graph $G = (\mathcal{V}, \mathcal{E})$, where $\mathcal{V} := \mathbb{N}_n$ is the set of vertices, and $\mathcal{E} \subset \mathcal{V} \times \mathcal{V}$ is the set of edges. Each vertex of the graph represents an agent. An edge from vertex $i \in \mathcal{V}$ to $j \in \mathcal{V}$ indicates that agents i and j can measure the relative position of each other in their local coordinate frames. In such a case, agents i and j are called neighbors. The set of neighbors of agent i is denoted by $\mathcal{N}_i := \{j \in \mathcal{V} \,|\, (i,j) \in \mathcal{E}\}$.

Throughout this work, we assume that the altitude of the UAVs are controlled separately, and the sensing topology among UAVs is fixed through all time. Furthermore, we assume that the UAVs move through an unobstructed airspace, where collision avoidance is not considered. In section VI we provide additional remarks on how to relax these assumptions and augment the control law to incorporate collision avoidance.

III. Formation Control for Single-integrator Agents

In this section, we present a distributed formation control strategy and a gain design approach based on optimization for agents with single-integrator dynamics. The results of this section are a cornerstone of the UAV control strategy discussed in the next section.

A. Control for Agents with Single-integrator Model

Consider n agents with the single integrator dynamics

$$\dot{q}_i = u_i, \qquad i \in \{1, 2, \ldots, n\}, \tag{1}$$

where $q_i := [x_i, y_i]^T \in \mathbb{R}^2$ is the coordinate of agent i in a common global coordinate frame (unknown to agents), and u_i is the control law, that we define as

$$u_i := \sum_{j \in \mathcal{N}_i} A_{ij}\,(q_j - q_i), \tag{2}$$

where $A_{ij} \in \mathbb{R}^{2\times 2}$ are constant control gain matrices to be determined. By constraining the gain matrices to the form

$$A_{ij} := \begin{bmatrix} a_{ij} & b_{ij} \\ -b_{ij} & a_{ij} \end{bmatrix}, \qquad a_{ij}, b_{ij} \in \mathbb{R}, \tag{3}$$

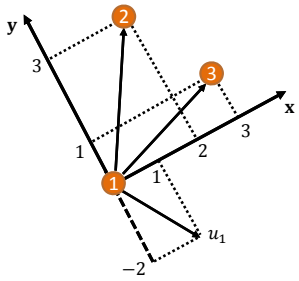

Fig. 2. Example of three agents with agents 2 and 3 neighbors of agent 1.

it can be shown that the closed-loop dynamics with coordinates q_i and q_j expressed in agents' local coordinate frames are identical to the case that coordinates are expressed in a common global frame (for more details see [12]). Therefore, while the implementation is distributed and uses the local relative position measurements, the control strategy can be designed and analyzed in a global coordinate frame. The geometric intuition behind the control strategy (2) is explained in the following example.

Example 1. Consider three agents in Fig. 2, where agents 2 and 3 are neighbors of agent 1. Let $q_2 = [2, 3]^\top$ and $q_3 = [3, 1]^\top$ denote the position of neighbors in agent 1's local coordinate frame, and assume that control gains for agent 1 are given as

$$A_{12} = \begin{bmatrix} 2 & -1 \\ 1 & 2 \end{bmatrix}, \qquad A_{13} = \begin{bmatrix} -1 & 3 \\ -3 & -1 \end{bmatrix}. \tag{4}$$

From (2), the control vector for agent 1 is computed as

$$u_1 = A_{12}\,q_2 + A_{13}\,q_3 = \begin{bmatrix} 1 \\ -2 \end{bmatrix}, \tag{5}$$

which is shown in the figure and can be interpreted geometrically as follows. At any instance of time, agent 1 moves along the control vector with the speed equal to the vector's magnitude. Note that due to the special structure of gain matrices A_{12}, A_{13}, they can be interpreted as scaled rotation matrices that rotate and scale vectors connecting agent 1 to its neighbors. One can see that this action is independent of agent 1's coordinate frame position and orientation, hence, q_1 and q_2 can replaced by their coordinates in a global coordinate frame.

Let $q := [q_1^\top, q_2^\top, \ldots, q_n^\top]^\top \in \mathbb{R}^{2n}$, and $u := [u_1^\top, u_2^\top, \ldots, u_n^\top]^\top \in \mathbb{R}^{2n}$ denote the aggregate state and control vectors of all agents, respectively. Using this notation, the closed-loop dynamics can be expressed as

$$\dot{q} = A\,q, \tag{6}$$

where

$$A = \begin{bmatrix} -\sum_{j=2}^{n} A_{1j} & A_{12} & \cdots & A_{1n} \\ A_{21} & -\sum_{\substack{j=1 \\ j\neq 2}}^{n} A_{2j} & \cdots & A_{2n} \\ \vdots & & \ddots & \vdots \\ A_{n1} & A_{n2} & \cdots & -\sum_{j=1}^{n-1} A_{nj} \end{bmatrix} \in \mathbb{R}^{2n\times 2n}, \tag{7}$$

is the aggregate state matrix that consists of A_{ij}'s, and has block Laplacian structure. Note that if $j \notin \mathcal{N}_i$, then A_{ij} in (7) is zero. Also, the 2×2 diagonal blocks are the negative sum of the rest of the blocks on the same row. From the block Laplacian structure of A, it follows that vectors

$$\begin{aligned} \mathbf{1} &:= [1,0,1,0,\ldots,1,0]^\top \in \mathbb{R}^{2n} \\ \bar{\mathbf{1}} &:= [0,1,0,1,\ldots,0,1]^\top \in \mathbb{R}^{2n} \end{aligned} \tag{8}$$

are in the kernel[1] of A.

Let $q^* \in \mathbb{R}^{2n}$ denote the coordinates of agents in an arbitrary embedding of the desired formation. That is, coordinates of agents at their desired formation in a coordinate frame that is chosen arbitrarily. Further, let $\bar{q}^* \in \mathbb{R}^{2n}$ be the coordinates of agents in this embedding when the formation is rotated by 90 degrees about the origin.

Theorem 1. *Consider a team of n single-integrator agents with closed-loop dynamics* (6)*. Assume that A is such that*

- *Vectors* $\mathbf{1}, \bar{\mathbf{1}}, q^*$ *and* $\bar{q}^*$ *are in the kernel of A,*
- *Other than the four zero eigenvalues associated with these eigenvectors, the remaining eigenvalues of A have negative real parts.*

Then, starting from any initial condition, agents converge to the desired formation up to a rotation, translation, and a non-negative scale factor.

Proof of Theorem 1 follows from the following Lemma, which is well-known from the linear systems theory (for more details on the proof see Theorem 1 in [12]).

Lemma 1. *Suppose that nonzero eigenvalues of A have negative real parts. Then, all trajectories of* $\dot{q} = Aq$ *exponentially converge to the kernel of A.*

The conclusion of Theorem 1 follows from Lemma 1 and noting that the kernel of A corresponds to all rotations, translations, and non-negative scale factors of the desired formation. We should point out that the kernel vectors $\mathbf{1}, \bar{\mathbf{1}}$ correspond to the case where all agents coincide, which can be considered as the desired formation achieved with the zero scale. Further, note that if agents are not initially coinciding, they will never converge to this coinciding equilibrium. To find a gain matrix that meets the conditions of the Theorem, one can formulate an optimization problem.

B. Formation Control With Fixed Scale

To fix the scale of the final formation, control law (2) can be augmented by a bounded smooth map $f : \mathbb{R} \to \mathbb{R}$ as

$$u_i = \sum_{j\in\mathcal{N}_i} A_{ij}(q_j - q_i) + f(d_{ij} - d_{ij}^*)(q_j - q_i), \tag{9}$$

where $d_{ij} := \|q_j - q_i\|$ denote the distance between agent i and j, $d_{ij}^* \in \mathbb{R}$ is its desired value, and f is chosen such that $x f(x) > 0$ for $x \neq 0$, and $f(0) = 0$. Possible choices for f are $f : x \mapsto \frac{1}{k}\arctan(x)$ or $f : x \mapsto \frac{1}{k}\tanh(x)$, where $k > 0$ is an arbitrary constant. The role of f in (9) is to pull agents toward their neighbors when the distance between them is larger than the desired value, and vice versa. By linearizing the closed-loop dynamics, it is straightforward to show that the desired formation is a *locally asymptotically* stable equilibrium. Furthermore, global stability of the system follows from the assumption that f is bounded. The study of *global asymptotic* stability of the desired formation requires additional analysis, and will be a topic of future work.

[1] If $A \in \mathbb{R}^{n\times n}$, the kernel or null space of A is defined as $\ker(A) := \{v \in \mathbb{R}^n \,|\, Av = 0\}$.

C. Control Gain Design via Optimization

Given a desired formation, we proceed by showing how a stabilizing gain matrix can be designed to meet the conditions of Theorem 1. Let q^* and $\bar{q}^*$ respectively denote the coordinates of agents in an arbitrary embedding of the desired formation and 90° rotated desired formation. Define $N := [q^*, \bar{q}^*, \mathbf{1}, \bar{\mathbf{1}}] \in \mathbb{R}^{2n\times 4}$, where $\mathbf{1}, \bar{\mathbf{1}}$ are given in (8). Notice that N is a set of bases for the kernal of A. Let $USV^\top = N$ be the (full) singular value decomposition (SVD) of N, where

$$U = [\bar{Q},\ Q] \ \in \mathbb{R}^{2n\times 2n}, \tag{10}$$

with $Q \in \mathbb{R}^{2n\times(2n-4)}$ defined as the last $2n-4$ columns of U.

Lemma 2. *Using Q in* (10)*, define*

$$\bar{A} := Q^\top A Q \ \in \mathbb{R}^{(2n-4)\times(2n-4)}. \tag{11}$$

Matrices A and $\bar{A}$ *have the same set of nonzero eigenvalues.*

Proof of Lemma 2 follows by observing that U is an orthogonal matrix, and $\text{range}(\bar{Q}) = \text{range}(N)$. Therefore $\bar{A}$ is the projection of A onto the orthogonal complement of $\text{range}(N)$. Effectively, the projection (11) removes the zero eigenvalues of A and allows us to formulate the stability of A in terms of $\bar{A}$.

Under the assumption that the sensing topology is undirected, gain matrices A and $\bar{A}$ are symmetric, and therefore their eigenvalues are real and can be ordered. In this case, a stabilizing gain matrix A is found by solving the optimization problem

$$\begin{aligned} A \ = \ \underset{a_{ij},\,b_{ij}}{\text{argmax}} \quad & \lambda_1(-\bar{A}) \\ \text{subject to} \quad & AN = 0 \end{aligned} \tag{12}$$

where $\lambda_1(\cdot)$ denote the smallest eigenvalue of a matrix. Note that problem (12) is convex [13], and can be formulated as the semidefinite programming (SDP) problem

$$\begin{aligned} A \ = \ \underset{a_{ij},\,b_{ij},\,\gamma}{\text{argmax}} \quad & \gamma \\ \text{subject to} \quad & \bar{A} + \gamma I \preceq 0 \\ & AN = 0 \end{aligned} \tag{13}$$

where the first constraint is a linear matrix inequality. In recent years, effective algorithms for numerically solving SDPs have been developed and are now available [14]. For our simulations, we used CVX [15], which is available free online, to solve problem (12). The proposed approach for finding stabilizing gain matrix A is summarized in Algorithm 1.

Algorithm 1: Formation control gain design.

input : Desired formation coordinates q^*.
output: Gain matrix A.

step 1: Let $N := [q^*, \bar{q}^*, \mathbf{1}, \bar{\mathbf{1}}]$.
step 2: Compute SVD of $N = USV^\top$.
step 3: Define Q as the last $2n-4$ columns of U.
step 4: Solve (12) using a SDP solver.

We point out that the optimization approach used here relies on a centralized paradigm and knowledge of the sensing topology. Once gains are computed, they can be transmitted to agents before the mission. Hence, agents can use the prescribed gains during the mission to achieve the desired formation without a need for communication. If agents can communicate, distributed optimization techniques can be used to solve (13) without relying on the complete knowledge of the sensing topology. An example of such distributed design can be found in [16].

IV. Formation Control for UAVs

In this section, we introduce the unicycle kinematic model with Dubins constraints, which provides a good description of the UAV's motion that is well suited for a high-level path planning autopilot control input. Based on this model, we develop a guidance strategy for UAVs such that they autonomously achieve a desired formation and travel along a straight line toward a desired destination.

We first propose a strategy without enforcing the Dubins constraints on the speed and rate of turn of aircrafts. We then extend the control to include the Dubins constraints. Throughout this section, we assume that the sensing graph is undirected, and a symmetric negative semi-definite control gain matrix A is designed for the desired formation by solving the optimization problem (12).

A. Unicycle Kinematic Model with Dubins Constraints

Under the assumption that the autopilot is tuned to set the airspeed and heading angle of a UAV to desired commanded values, the unicycle kinematic model

$$\begin{aligned} \dot{x}_i &= v_i \cos(\theta_i) \\ \dot{y}_i &= v_i \sin(\theta_i) \\ \dot{\theta}_i &= \omega_i \end{aligned} \tag{14}$$

provides a good description of the UAV's motion at a constant altitude. In (14), $x_i, y_i \in \mathbb{R}$ are coordinates of agent i, and $\theta_i \in [0, 2\pi)$ is the heading (or yaw) angle with respect to a global coordinate frame. Scalars $v_i \in \mathbb{R}$ and $\omega_i \in \mathbb{R}$ are respectively the linear and angular velocities of the UAV. A schematic of UAV at the mentioned coordinate is illustrated in Fig. 3.

Physical capabilities of the UAV limits the achievable airspeed and heading angles that can be commanded. These physical limits can be represented by the constraints

$$\begin{aligned} v_{\min} \;\le\; v_i \;\le\; v_{\max}, \\ |\omega_i| \;\le\; \omega_{\max}, \end{aligned} \tag{15}$$

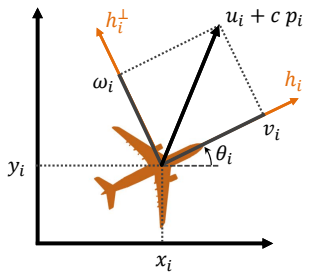

Fig. 3. Agent i at position $[x_i, y_i]^\top$ in the global coordinate frame. The agent's heading vector h_i makes angles θ_i with the x-axis. Linear and angular velocities v_i and ω_i are defined as projections of the control vector $u_i + c\,p_i$ on h_i and $h_i^\perp$ axes, respectively.

where $v_{\max} > v_{\min} > 0$ and $\omega_{\max} > 0$ are positive real scalars. Note that under theses constraints, the minimum turn radius of UAV is given by $R_{\min} = \frac{v_{\min}}{\omega_{\max}}$.

Input constraints (15), together with the kinematic model (14), are referred to as the Dubins unicycle kinematic model [17]. Note that this model does not include aerodynamics, wind effects, disturbances, etc., and is not sufficiently accurate for low-level autopilot design, however, it is well suited for a high level path planning and path following control design. A comprehensive discussion of aircraft dynamic models can be found in [18]–[22].

To derive an alternative formulation for (14) that is more suitable for the formation control design, we define the heading vector $h_i \in \mathbb{R}^2$ and its perpendicular vector $h_i^\perp \in \mathbb{R}^2$ as

$$h_i := \begin{bmatrix} \cos(\theta_i) \\ \sin(\theta_i) \end{bmatrix}, \qquad h_i^\perp := \begin{bmatrix} -\sin(\theta_i) \\ \cos(\theta_i) \end{bmatrix}. \tag{16}$$

Seeing that $\dot{h}_i = h_i^\perp \dot{\theta}_i$, we can describe the dynamics (14) equivalently by

$$\begin{aligned} \dot{q}_i &= h_i v_i \\ \dot{h}_i &= h_i^\perp \omega_i. \end{aligned} \tag{17}$$

Let $q := [q_1^\top, q_2^\top, \ldots, q_n^\top]^\top \in \mathbb{R}^{2n}$ be the aggregate position vector of all UAVs, and similarly let $h \in \mathbb{R}^{2n}$, $v \in \mathbb{R}^n$, $\omega \in \mathbb{R}^n$ be the aggregate heading, linear velocity, and angular velocity vectors, respectively. Using this notation, the motion of UAVs can be collectively expressed as

$$\begin{aligned} \dot{q} &= H v \\ \dot{h} &= H^\perp \omega, \end{aligned} \tag{18}$$

where matrices $H, H^\perp \in \mathbb{R}^{2n \times n}$ are defined as

$$H = \begin{bmatrix} h_1 & 0 & \cdots & 0 \\ 0 & h_2 & & 0 \\ \vdots & & \ddots & \vdots \\ 0 & 0 & \cdots & h_n \end{bmatrix}, \quad H^\perp = \begin{bmatrix} h_1^\perp & 0 & \cdots & 0 \\ 0 & h_2^\perp & & 0 \\ \vdots & & \ddots & \vdots \\ 0 & 0 & \cdots & h_n^\perp \end{bmatrix}. \tag{19}$$

B. Formation Control Without Input Constraints

Consider a team of UAVs with dynamics (18). We seek to assign guidance strategies v and ω to the UAVs such that they autonomously achieve a desired formation and

travel toward a desired destination. To simplify the analysis, which can help with understanding the underlying idea of the formation control design, we ignore Dubins constraints (15). These constraints will be taken into account in the following subsection.

Let $p_i \in \mathbb{R}^2$ be a constant unit vector that the i'th UAV should travel along to reach the desired destination. Further, let $A \in \mathbb{R}^{2n\times 2n}$ be a symmetric gain matrix designed in Section III-C for agents with single-integrator model to achieve the desired formation. Denote by $u_i = \sum_{j\in\mathcal{N}_i} A_{ij}(q_j - q_i)$ the desired holonomic control direction for agent i. The proposed control strategy for UAVs is as follows. Each UAV computes the control vector $u_i + c\,p_i$, where $c > 0$ is a constant desired speed. The projections of this vector along the heading direction h_i and its perpendicular vector $h_i^\perp$ are then calculated and used as the linear and angular velocity commands, respectively. Specifically, the linear and angular velocity control are given by

$$\begin{aligned} v_i &:= h_i^\top (u_i + c\,p_i) \\ \omega_i &:= h_i^{\perp\top}(u_i + c\,p_i), \end{aligned} \tag{20}$$

as illustrated in Fig. 3.

Theorem 2. *Let A be a symmetric gain matrix designed for agents with single-integrator model, $c > 0$, and assume that p_i's are constant and identical for all agents. Under the control* (20)*, UAVs converge to the desired formation and travel along the direction p with speed c.*

Proof of Theorem 2 is given in the Appendix. Note that for p_i's to be identical, the agents' local coordinate frames do not need to be aligned. That is, p_i can be provided to an agent with respect to its local coordinate frame.

C. Formation Control With Input Constraints

We now present a modified guidance strategy for UAVs that incorporates the Dubins constraints (15). Given the unconstrained control (20), we define the saturated control as

$$\begin{aligned} v_i &:= \bar{s}_i\left(s_i(h_i^\top u_i) + c\,h_i^\top p_i\right) \\ \omega_i &:= r_i\left(r_i(h_i^{\perp\top} u_i) + c\,h_i^{\perp\top} p_i\right), \end{aligned} \tag{21}$$

with saturation functions $\bar{s}_i, s_i, r_i : \mathbb{R} \to \mathbb{R}$ defined as

$$s_i(x) = \begin{cases} x & \text{if } |x| \le u_{\max} \\ \frac{u_{\max}}{|x|} & \text{if } |x| > u_{\max} \end{cases}, \tag{22}$$

$$\bar{s}_i(x) = \begin{cases} v_{\min} & \text{if } x \le v_{\min} \\ x & \text{if } v_{\min} \le x \le v_{\max} \\ v_{\max} & \text{if } v_{\max} \le x \end{cases}, \tag{23}$$

and

$$r_i(x) = \begin{cases} x & \text{if } |x| \le \omega_{\max} \\ \frac{\omega_{\max}}{|x|} & \text{if } |x| > \omega_{\max}. \end{cases} \tag{24}$$

Based on extensive numerical simulations, we conjecture that under the control (21), if $u_{\max} := \frac{v_{\max}-v_{\min}}{2}$ and $v_{\min} \le c \le v_{\max}$, UAVs converge to the desired formation while moving at the desired speed toward the destination. Proof of convergence for the proposed strategy is a topic of future work.

V. Simulations

To validate the proposed strategy, simulations with desired formations defined as a triangle and a square are performed. For each formation, the saturated UAV control law (21) with u_i given by (2) and (9) are considered. The dynamics of the UAVs used in the simulations is given by (14) and (15). The minimum and maximum speed of all UAVs are set to $v_{\min} = 3$ m/s and $v_{\max} = 5$ m/s, and the heading angle rate of change is limited by $\omega_{\max} = \frac{\pi}{4}$. The desired direction of travel for all agents is set along the positive x-axis of the (unknown to agents) world coordinate frame, i.e., $p_i = [1, 0]^\top$. Links to simulation code and video are provided in the Supplementary Material section.

A. Triangle Formation

In the first set of simulations, the desired formation is defined as a triangle formation, as illustrated in Fig. 1, where the sensing graph among six UAVs is shown by gray lines connecting the agents. Notice that this sensing graph is undirected, and we assume that it is fixed through the simulation. Stabilizing control gains associated to this desired formation are computed from the optimization routine explained in Section III-C.

In the first simulation, u_i given by (2) is considered, and the initial position and heading of the UAVs are chosen randomly as shown in Fig. 4(a) at time $t = 0$s. The location of UAVs at other instances of time are shown in Figs. 4(b)-(e). As can be seen, the proposed control strategy navigate the UAVs to the desired formation and set their headings toward the desired direction. Notice that since the formation controller only uses the local relative position measurements, the desired formation is achieved up to a rotation and translation. That is, the orientation of the triangle formation is not controlled. This can be seem by comparing Figs. 1 and 4(e). Moreover the scale of the formation achieved in Fig. 4(e) is not controlled, and depends on the starting position of the agents. In this case, the distance between each agent and its neighbors is equal to 14 m.

In the next simulation, augmented control law (9) is used instead to fix the scale of the formation. In (9), the map f is defined as $f(x) = \arctan(x)$, and the desired distance between an agent and its neighbors is defined as $d_{ij}^* := 10$ m. The initial condition of UAVs is chosen the same as previous simulation to allow better comparison, and is shown in Fig. 5(a) at $t = 0$s. The location of UAVs at identical instances of time to Fig. 4 are shown in Figs. 5(b)-(e). As can be seen, the proposed control strategy brings the UAVs to the desired formation and set their headings toward the desired direction. Furthermore, the distance between the UAVs reaches the desired value of 10 m.

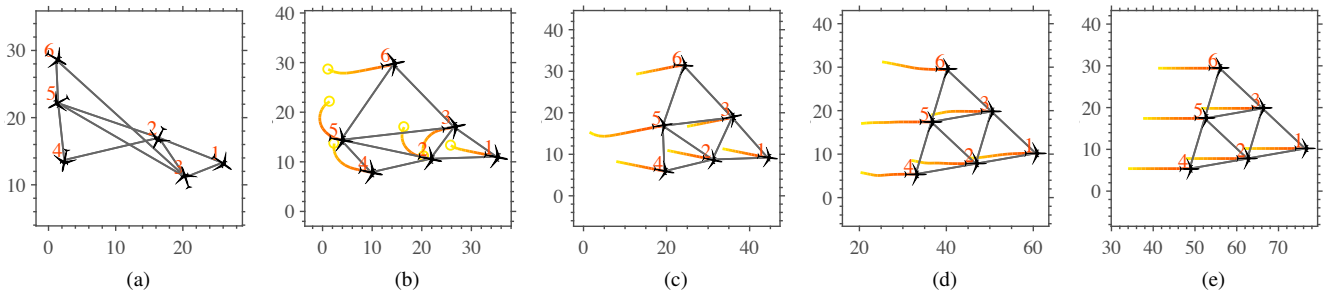

Fig. 4. Simulation of 6 UAVs starting from a random initial pose and achieving a triangle formation while traveling along toward the positive x-axis. (a) Initial pose at $t = 0$s. (b) $t = 31$s. (c) $t = 63$s. (d) $t = 102$s. (e) $t = 142$s.

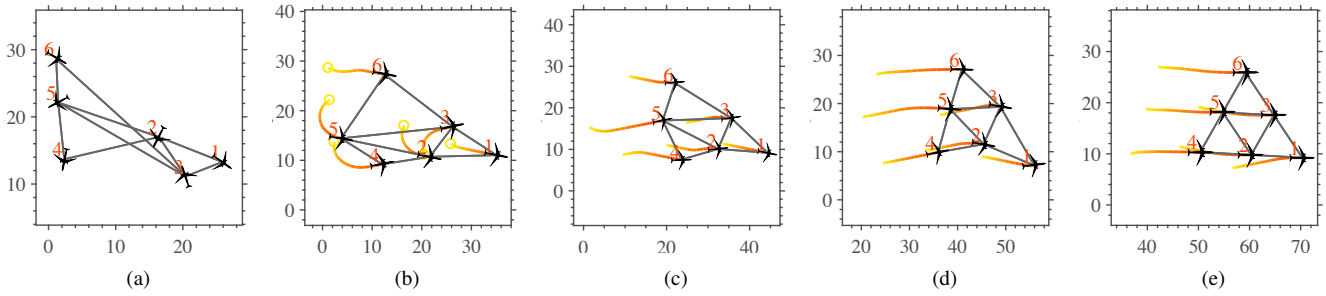

Fig. 5. Simulation of 6 UAVs starting from a random initial pose and achieving a triangle formation with *fixed* scale while traveling along toward the positive x-axis. (a) Initial pose at $t = 0$s. (b) $t = 31$s. (c) $t = 63$s. (d) $t = 102$s. (e) $t = 142$s.

B. Square Formation

In the second set of simulations, the desired formation is defined as a square grid with nine UAVs. This formation, and the sensing graph among UAVs can be see in Fig. 7(e). Stabilizing control gains associated to this desired formation are computed from the optimization routine explained in Section III-C.

In the first simulation, u_i given by (2) is used, and initial position and heading of UAVs are chosen randomly as shown in Fig. 6(a) at $t = 0$s. The location of UAVs at other instances of time are shown in Figs. 6(b)-(e). As can be seen, the proposed control strategy navigate the UAVs to the desired formation and set their headings toward the desired direction. The distance between each agent and its neighbors in the final formation is equal to 3.8 m.

To fix the scale of the formation, augmented control law (9) is used in the next simulation, where $f(x) = \arctan(x)$, and the desired distance between an agent and its neighbors is defined as $d_{ij}^* := 10$ m. The initial condition of UAVs is chosen as before, and is shown in Fig. 7(a). The location of UAVs at subsequent instances of time are shown in Figs. 7(b)-(e), where as can be seen, the proposed control strategy navigate the UAVs to the desired formation and set their headings toward the desired direction. The distance between the UAVs at the final formation reaches the desired value of 10 m.

VI. Concluding Remarks and Future Work

We presented a distributed formation control strategy for a team of UAVs to autonomously achieve and maintain a desired formation while traveling toward a desired destination. Given a desired formation, we showed how stabilizing control gains can be found from solving a convex optimization problem. These gains, which can be communicated to the agents before start of the mission, were used to calculate linear and angular velocity control commands for the UAVs under the Dubins constraint. Simulations were provided to show that under the proposed control the UAVs achieve the desired formation and travel along the assigned direction. Proof of convergence for the saturated UAV control is a topic of future work.

To preserve connectivity, avoid obstacles, or prevent collision among UAVs, distributed techniques such as potential field [23], [24], traffic circle [25], or control barrier function [26] approach can be employed. Another strategy is a temporary change of altitude, i.e., UAVs passing over or under each other to avoid collision. This strategy can preserve the stability properties, however, the low-level altitude controller can become more complicated. Incorporating collision/obstacle avoidance strategies with the proposed formation control and analyzing the stability properties of the resulting system will be a topic of future work.

Lastly, we assumed that the inter-agent sensing topology is fixed through all time. Strategies such as [12] can be deployed when the sensing topology is time-varying or switching.

Appendix

A. Proof of Theorem 2

Proof. Let us denote by $p := [p_1^\top, p_2^\top, \ldots, p_n^\top]^\top \in \mathbb{R}^{2n}$ the aggregate desired direction vector. From (20), the control

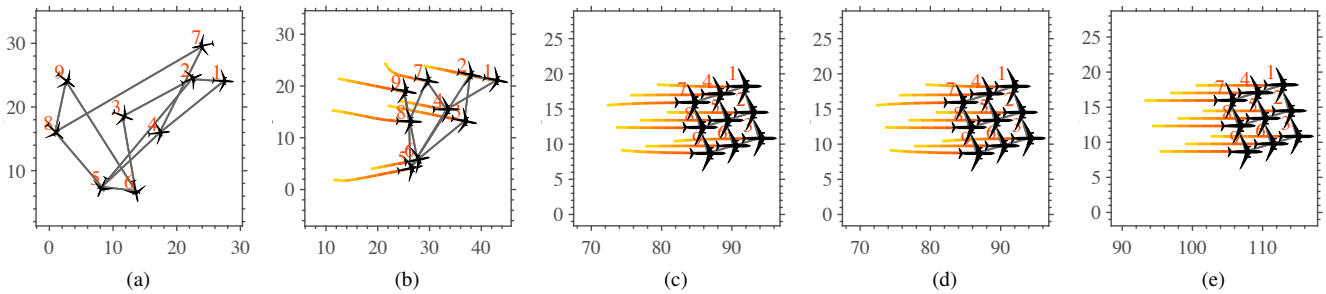

Fig. 6. Simulation of 9 UAVs starting from a random initial pose and achieving a square formation while traveling along toward the positive x-axis. (a) Initial pose at $t = 0$s. (b) $t = 52$s. (c) $t = 100$s. (d) $t = 192$s. (e) $t = 245$s.

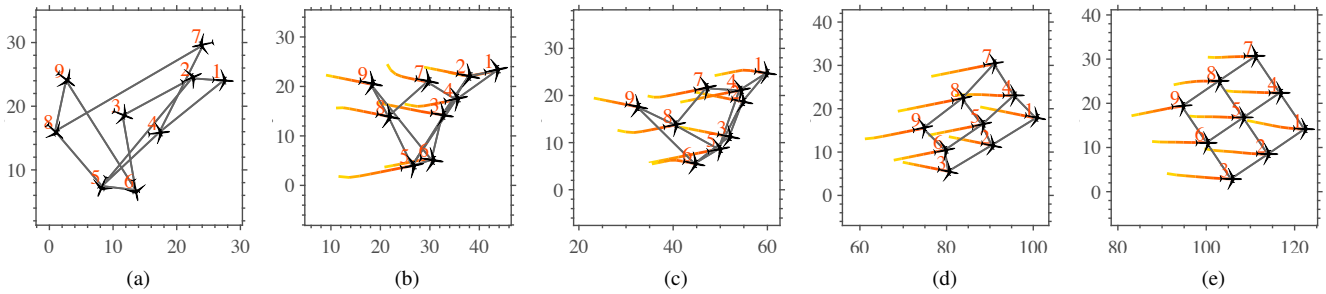

Fig. 7. Simulation of 9 UAVs starting from a random initial pose and achieving a square formation with *fixed* scale while traveling along toward the positive x-axis. (a) Initial pose at $t = 0$s. (b) $t = 52$s. (c) $t = 100$s. (d) $t = 192$s. (e) $t = 245$s.

for all agents can be expressed in the vector form as

$$\begin{aligned} v &= H^\top (Aq + cp), \\ \omega &= H^{\perp\top} (Aq + cp) \end{aligned} \tag{25}$$

where H and $H^\perp$ are defined in (19). Under the proposed control, the closed-loop dynamics is given by replacing (25) in (18) as

$$\begin{aligned} \dot{q} &= HH^\top (Aq + cp), \\ \dot{h} &= H^\perp H^{\perp\top} (Aq + cp). \end{aligned} \tag{26}$$

Let $q^* \in \mathbb{R}^{2n}$ be the coordinates of agents in an arbitrary embedding of the desired formation. One can see that

$$\begin{aligned} q(t) &= q^* + tcp \\ h(t) &= p \end{aligned} \tag{27}$$

satisfies the dynamics (26), and therefore is a relative equilibrium. This can be verified by replacing (27) in (26), and noting that q^* is in the kernel of A, i.e., $Aq^* = 0$. Furthermore, $Ap = 0$ since A has Laplacian structure and by assumption unit vectors p_i are all identical. Note that the relative equilibrium (27) corresponds to UAVs traveling in formation along the desired direction p. Consider the change of variable $\bar{q} = q - tcp$. Replacing q by $\bar{q} + tcp$ in (26), and noting that $Ap = 0$, and $HH^\top - I = -H^\perp H^{\perp\top}$, yields the dynamics

$$\begin{aligned} \dot{\bar{q}} &= HH^\top A\bar{q} - H^\perp H^{\perp\top} cp \\ \dot{h} &= H^\perp H^{\perp\top} (A\bar{q} + cp). \end{aligned} \tag{28}$$

Consider the Lyapunov function candidate

$$V := -\frac{1}{2}\bar{q}^\top A\bar{q} + \frac{c}{2}(h-p)^\top (h-p) \ \geq 0. \tag{29}$$

Since p is a constant vector and $h^\top H^\perp = 0$, the derivative of V along the trajectories of (28) is

$$\begin{aligned} \dot{V} &= -\bar{q}^\top A\dot{\bar{q}} + c(h-p)^\top \dot{h} \\ &= -\bar{q}^\top AHH^\top A\bar{q} + c\bar{q}^\top AH^\perp H^{\perp\top} p \\ &\qquad + c(h-p)^\top H^\perp H^{\perp\top} (A\bar{q} + cp) \\ &= -\bar{q}^\top AHH^\top A\bar{q} + c\bar{q}^\top AH^\perp H^{\perp\top} p \\ &\qquad - cp^\top H^\perp H^{\perp\top} A\bar{q} - c^2 p^\top H^\perp H^{\perp\top} p \\ &= -\bar{q}^\top AHH^\top A\bar{q} - c^2 p^\top H^\perp H^{\perp\top} p \\ &= -\left(H^\top A\bar{q}\right)^\top \left(H^\top A\bar{q}\right) - \left(cH^{\perp\top} p\right)^\top \left(cH^{\perp\top} p\right) \\ &= -\|H^\top A\bar{q}\|^2 - \|cH^{\perp\top} p\|^2 \ \leq 0 \end{aligned} \tag{30}$$

which implies that the system is stable. To show convergence to desired heading, from $\dot{V} = 0$ we have that $H^{\perp\top} p = 0$, which implies $h_i^{\perp\top} p_i = 0$ for all i. Since the case $h_i = -p_i$ is excluded by (27), we conclude that $h_i = p_i$, i.e., agents fly along the desired direction. To show convergence to the desired formation, from $\dot{V} = 0$ we show that $\bar{q}$ is in the kernel of A. Indeed, $\dot{V} = 0$ implies that $H^\top A\bar{q} = 0$, and by LaSalle's invariance principle, $\bar{q}$ converges to the largest invariant set in $\{\bar{q} \in \mathbb{R}^{2n} \,|\, H^\top A\bar{q} \equiv 0\}$. Thus, one of the following cases must hold:

(i) $A\bar{q} \equiv 0$
(ii) $A\bar{q} \not\equiv 0$, $H^\top A\bar{q} \equiv 0$

For case (i), from (28) we get $\dot{\bar{q}} \equiv \dot{h} \equiv 0$, which implies that the desired formation is achieved and is an invariant set. We now show that case (ii) cannot happen. In this case, $H^\top A\bar{q} \equiv 0$ implies that there exists constants $c_1, c_2, \ldots, c_n \in \mathbb{R}$, with

at least one $c_i \neq 0$, such that

$$A\bar{q} = \begin{bmatrix} c_1 h_1^{\perp} \\ c_2 h_2^{\perp} \\ \vdots \\ c_n h_n^{\perp} \end{bmatrix}. \tag{31}$$

Since $H^{\top} A\bar{q} \equiv 0$, from (28) we get $\dot{q} \equiv 0$. Thus, $\bar{q}$ and $A\bar{q}$ are constant, and from (31) we conclude that $h_i^{\perp}$ (and thus h_i) is constant for all nonzero c_i. From the definition of $H^{\perp}$ in (19), one can see that $H^{\perp}$ has full column rank. Therefore, it does not have a right null vector, and since from (31) we have $H^{\perp\top} A\bar{q} \neq 0$, we get $H^{\perp} H^{\perp\top} A\bar{q} \neq 0$. Consequently, from (28) we get $\dot{h} \neq 0$, which implies that the heading vectors are not fixed and rotating. This is a contradiction and shows that case (ii) cannot happen. □

REFERENCES

[1] P. Rudol and P. Doherty, "Human body detection and geolocalization for uav search and rescue missions using color and thermal imagery," in *Aerospace Conference*. IEEE, 2008, pp. 1–8.

[2] M. A. Goodrich, B. S. Morse, D. Gerhardt, J. L. Cooper, M. Quigley, J. A. Adams, and C. Humphrey, "Supporting wilderness search and rescue using a camera-equipped mini uav," *Journal of Field Robotics*, vol. 25, no. 1-2, pp. 89–110, 2008.

[3] K. M. Fornace, C. J. Drakeley, T. William, F. Espino, and J. Cox, "Mapping infectious disease landscapes: unmanned aerial vehicles and epidemiology," *Trends in parasitology*, vol. 30, no. 11, pp. 514–519, 2014.

[4] J. Zhang, J. Hu, J. Lian, Z. Fan, X. Ouyang, and W. Ye, "Seeing the forest from drones: Testing the potential of lightweight drones as a tool for long-term forest monitoring," *Biological Conservation*, vol. 198, pp. 60–69, 2016.

[5] J. Scherer and B. Rinner, "Persistent multi-uav surveillance with energy and communication constraints," in *International Conference on Automation Science and Engineering*. IEEE, 2016, pp. 1225–1230.

[6] M. Owen, R. W. Beard, and T. W. McLain, "Implementing dubins airplane paths on fixed-wing uavs," in *Handbook of Unmanned Aerial Vehicles*. Springer, 2015, pp. 1677–1701.

[7] Z. Lin, L. Wang, Z. Han, and M. Fu, "Distributed formation control of multi-agent systems using complex laplacian," *IEEE Transactions on Automatic Control*, vol. 59, no. 7, pp. 1765–1777, July 2014.

[8] Z. Lin, L. Wang, Z. Han, and M. F. , "A graph laplacian approach to coordinate-free formation stabilization for directed networks," *IEEE Transactions on Automatic Control*, vol. 61, no. 5, pp. 1269–1280, May 2016.

[9] S. Zhao, D. V. Dimarogonas, Z. Sun, and D. Bauso, "A general approach to coordination control of mobile agents with motion constraints," *IEEE Transactions on Automatic Control*, 2017.

[10] S. Zhao, "Affine formation maneuver control of multi-agent systems," *IEEE Transactions on Automatic Control*, 2018.

[11] K. Fathian, D. I. Rachinskii, M. W. Spong, and N. R. Gans, "Globally asymptotically stable distributed control for distance and bearing based multi-agent formations," in *American Control Conference*. IEEE, 2016, pp. 4642–4648.

[12] K. Fathian, D. I. Rachinskii, T. H. Summers, M. W. Spong, and N. R. Gans, "Distributed formation control under arbitrarily changing topology," in *American Control Conference*. IEEE, 2017, pp. 271–278.

[13] S. Boyd, "Convex optimization of graph laplacian eigenvalues," in *Proceedings of the International Congress of Mathematicians*, vol. 3, no. 1-3, 2006, pp. 1311–1319.

[14] R. H. Tütüncü, K.-C. Toh, and M. J. Todd, "Solving semidefinite-quadratic-linear programs using sdpt3," *Mathematical programming*, vol. 95, no. 2, pp. 189–217, 2003.

[15] M. Grant and S. Boyd, "CVX: Matlab software for disciplined convex programming, version 2.1," http://cvxr.com/cvx, Mar. 2014.

[16] Z. Lin, L. Wang, Z. Chen, M. Fu, and Z. Han, "Necessary and sufficient graphical conditions for affine formation control," *Transactions on Automatic Control*, vol. 61, no. 10, pp. 2877–2891, 2016.

[17] H. Chitsaz and S. M. LaValle, "Time-optimal paths for a dubins airplane," in *Conference on Decision and Control*. IEEE, 2007, pp. 2379–2384.

[18] R. C. Nelson, *Flight stability and automatic control*. WCB/McGraw Hill New York, 1998, vol. 2.

[19] T. R. Yechout, *Introduction to aircraft flight mechanics*. AIAA, 2003.

[20] W. F. Phillips, *Mechanics of flight*. John Wiley & Sons, 2004.

[21] R. W. Beard and T. W. McLain, *Small Unmanned Aircraft: Theory and practice*. Princeton university press, 2012.

[22] B. L. Stevens, F. L. Lewis, and E. N. Johnson, *Aircraft control and simulation: dynamics, controls design, and autonomous systems*. John Wiley & Sons, 2015.

[23] A. C. Satici, H. Poonawala, H. Eckert, and M. W. Spong, "Connectivity preserving formation control with collision avoidance for nonholonomic wheeled mobile robots," in *International Conference on Intelligent Robots and Systems*. IEEE, 2013, pp. 5080–5086.

[24] J. Jin, Y. Kim, S. Wee, D. Lee, and N. Gans, "A stable switched-system approach to collision-free wheeled mobile robot navigation," *Journal of Intelligent & Robotic Systems*, vol. 86, no. 3-4, pp. 599–616, 2017.

[25] J. Jin, Y.-G. Kim, S.-G. Wee, and N. Gans, "Decentralized cooperative mean approach to collision avoidance for nonholonomic mobile robots," in *International Conference on Robotics and Automation*. IEEE, 2015, pp. 35–41.

[26] L. Wang, A. D. Ames, and M. Egerstedt, "Multi-objective compositions for collision-free connectivity maintenance in teams of mobile robots," in *Conference on Decision and Control*. IEEE, 2016, pp. 2659–2664.